On the Draupner freak wave

Francesco Fedele*

School of Civil and Environmental Engineering, School of Electrical and Computer Engineering,

Georgia Institute of Technology, Atlanta, GA, USA.

**Corresponding author address:* Georgia Institute of Technology Atlanta, GA 30332, USA.

E-mail: fedele@gatech.edu

ABSTRACT

In this paper, we revisit extreme wave statistics related to the 1993's Draupner freak wave event drawing on ERA-interim reanalysis data. In particular, we study the influence of nonlinear wave-wave interactions and space-time variability of the wave field on the predictions of the maximum wave and crest heights expected at the Draupner site.

According to Janssen's (2003) theory, in realistic oceanic storms characterized by short-crested seas the wave field forgets its initial conditions and adjusts to a non-Gaussian state dominated by second order bound nonlinearities on time scales $t \gg t_c \approx 0.13T_0/\nu\sigma_\theta$ where T_0, ν and σ_θ denote mean wave period, spectral bandwidth and angular spreading of dominant waves respectively. In this regime, we propose that statistical predictions of extreme waves can be based on the Tayfun (1980) model combined with Adler-Taylor's (2009) theory on Euler-Characteristics of random fields.

According to ERA-interim reanalysis of the Draupner storm, it is found that $t_c/T_0 \sim O(1)$, indicating that quasi-resonant interactions are ineffective in amplyfing waves. Further, the probability that a wave with crest-to-trough height $H/H_s > 2.15$ occurs over the platform's area is roughly 10-50 times larger than the probability that the same wave is observed at a single point, where the significant wave height $H_s = 4\sigma$ and σ is the standard deviation of surface elevations. The analysis predicts that the associated second order nonlinear crest height exceeds the threshold $1.45H_s$, in fair agreement with measurements. These studies provide evidence that freak wave behavior may be a manifestation of the space-time properties of oceanic fields. The proposed theoretical framework can be applied to refine the predictions of higher resolution forecast wave models.

1. Introduction

The Draupner wave was recorded on 1 January 1995 by a downward pointing laser at the Draupner platform in the North Sea at a water depth $d = 70$ m (Haver (2001)). The freak wave occurred during a 5-hour sea state with significant wave height $H_s = 4\sigma = 11.9$ m, mean period $T_0 = 13.1$ s and wavelength $L_0 = 260$ m, and σ is the standard deviation of surface elevations. The crest height $h = 18.5$ m ($h/H_s = 1.55$) and the crest-to-trough height $H = 25.6$ m ($H/H_s = 2.15$) (Haver (2004); Karin Magnusson and Donelan (2013)). The wave profile was very steep, but there is no evidence that the wave was breaking. In the last decade the properties of the Draupner wave have been extensively studied (see Dysthe et al. (2008); Osborne (2010) and references therein). Several physical mechanisms have been proposed to explain the occurrence of such a giant wave (Kharif and Pelinovsky (2003)) including the two competing hypotheses of nonlinear focusing due to third-order wave-wave quasi-resonant interactions (Janssen (2003)) and purely dispersive focusing of second order waves (Fedele and Tayfun (2008); Fedele (2008)).

Third-order quasi-resonant interactions and associated modulational instabilities cause the statistics of weakly nonlinear gravity waves to significantly differ from the Gaussian structure of linear seas (Janssen (2003); Fedele (2008); Onorato et al. (2009); Shemer and Sergeeva (2009); Toffoli et al. (2010)), especially in long-crested seas. The wave field near a large crest is that of a breather (Peregrine (1983); Osborne et al. (2000), see also Ankiewicz et al. (2009)). One integral statistics used as a measure of the relative importance of such nonlinearities and the increased occurrence of large breathers is the excess kurtosis as defined by Janssen (2003) as

$$C_4 = \frac{\langle \eta^4 \rangle}{3\langle \eta^2 \rangle^2} - 1,$$

where η is the wave surface elevation, brackets denote statistical average and the fourth order cumulant $\mu_{40} = 3C_4$. In general, C_4 comprises a dynamic component due to nonlinear wave-

wave interactions (Janssen (2003)) and a bound contribution induced by the characteristic crest-trough asymmetry of ocean waves (Tayfun (1980); Tayfun and Lo (1990); Tayfun and Fedele (2007); Fedele and Tayfun (2008); Fedele (2008)). For long-crested seas at deep water, within the framework of the higher order compact Zakharov (cDZ) equation (Dyachenko and Zakharov (2011)), Fedele (2014a) showed that, correct to $O(\nu^2)$ in spectral bandwidth, the dynamic excess kurtosis monotonically increases to the asymptotic value

$$C_4^{cDZ} = C_4^{NLS}\left(1 - \frac{4\sqrt{3}+\pi}{8\pi}\nu^2\right) \approx C_4^{NLS}\left(1 - 0.40\nu^2\right),$$

where

$$C_4^{NLS} = BFI^2 \frac{\pi}{3\sqrt{3}} \tag{1}$$

is the dynamic excess kurtosis of long-crested or unidirectional narrowband waves described by one-dimensional (1-D) nonlinear Schrodinger (NLS) and Dysthe (1979) equations (Mori and Janssen (2006)), and the Benjamin-Feir index $BFI = \sqrt{2}\mu/\nu$, with μ denoting an integral measure of wave steepness and ν is the spectral bandwidth. Clearly, C_4^{cDZ} is smaller than C_4^{NLS}, especially as the spectral bandwidth widens. This is consistent with the result that in accord with cDZ the linear growth rate of a subharmonic perturbation reduces with respect to the NLS counterpart as wave steepness increases (Fedele (2014a)). Indeed, modulation instability is attenuated as μ increases, a well known result (Lighthill (1965)). Thus, we see that the occurrence of rogue waves induced by large breathers becomes less likely as the steepness of carrier wave increases. To date higher-order breathers have been observed experimentally only at sufficiently small values ($\sim 0.01 - 0.09$) of wave steepness (Chabchoub et al. (2011, 2012)) since wave breaking is inevitable for $\mu > 0.1$, as pointed out by Shemer and Alperovich (2013) (see also Shemer and Liberzon (2014)). They also noted that 'breather does not breath' and differs from the 1-D NLS solution due to significant asymmetric spectral widening. Moreover, breather amplification is smaller than that predicted by the NLS, indicating that modulation instability attenuates as waves steepen, in accord with the numerical studies of Euler equations (Slunyaev and Shrira (2013); Slunyaev et al. (2013)). Clearly, the preceding results are valid for unidirectional waves where energy is 'trapped' as in a long waveguide. If dissipation is negligible and the wave steepness is small, quasi-resonant interactions are effective in reshaping the wave spectrum, inducing nonlinear focusing via modulation instability before breaking occurs (Onorato et al. (2009); Chabchoub et al. (2011, 2012)). However, such 1-D conditions never occur in nature as they are unrealistic models of oceanic wind seas. These are typically short-crested and nonlinear focusing due to modulational effects is reduced since energy can spread directionally (Onorato et al. (2009); Toffoli et al. (2010)).

Recent studies also proposed the hypothesis that the Draupner wave occurred in crossing seas (Onorato et al. (2010)). The analytical study suggests that angles $\sim 10° - 30°$ between the dominant sea directions are the most probable for establishing a freak wave sea induced by quasi-resonant wave-wave interactions. However, Adcock et al. (2011) reported that the hindcast from the European Centre for Medium-Range Weather Forecasts shows swell waves propagating at approximately 80° to the wind sea. Adcock et al. (2011) also argued that the Draupner wave occurred due to crossing of two almost orthogonal wave-groups in accord with second order theory. This explains the large set-up observed under the giant wave instead of the expected set-down. However, there is no evidence of significant swell components nearby the platform as clearly seen from Fig. 2 in Adcock et al. (2011) and Fig. 1, which shows the ERA-interim wave directional spectrum at the Draupner site. Clearly, one can also argue that the observed set-up is an indication that measurements may be corrupted. Further, in accord with Boccotti's (2000) quasi-determinism theory the probability that two different wave groups cross at the same point at the apex of their development is much smaller than the probability that one of the two groups focuses at the same point .

The sea state of the Draupner wave was short-crested (see Fig. 1 and bottom-right panel of Fig. 2) and occurred on finite depth ($d/L_0 \sim 0.3$) where modulation instabilities are attenuated and thus may have played an insignificant role in the wave growth. Recently, Tayfun (2008) arrived at similar conclusions based on the analysis of North Sea data. His results indicate that large *time waves* (measured at a given point) result from the constructive interference (focusing) of elementary waves with random amplitudes and phases enhanced by second-order non-resonant interactions. Further, the surface statistics is not affected by third-order nonlinearities, and it obeys the Tayfun distribution (Tayfun (1980); Fedele and Tayfun (2008)) in agreement with observations (Fedele (2008)). This is confirmed by a recent quality data control and analysis by Christou and Ewans (2014) of single-point field measurements from fixed sensors mounted on offshore platforms, the majority of which were recorded in the North Sea. The analysis of an ensemble of 122 million individual waves revealed 3649 rogue events, concluding that freak waves observed at a point in time, i.e. *time waves*, are merely rare events induced by dispersive focusing.

Furthermore, recent studies by Fedele (2012) and Fedele et al. (2013) provided both theoretical and experimental evidences that the expected maximum wave surface height over an area in time (*space-time extreme*) is larger than that expected at a fixed point (*time extreme*), especially in short-crested seas (see also Forristall (2011)). Indeed, the occurrence of an extreme in Gaussian fields is analogous to that of a big wave that a surfer is in search and always finds (Baxevani and Rychlik (2006)). If he spans a large area the chances to encounter the largest crest of a wave group increase (Rosenthal and Lehner (2008)).

The preceding provide the principal motivation for revisiting the Draupner's event and study the space-time properties of the sea state in which the freak wave occurred. The remainder of the paper is organized as follows. First, the essential elements of Janssen's formulation for the excess kurtosis of directional or short-crested seas are presented (Fedele (2014b)). This is followed by a review of the essential elements of the theory of Euler Characteristics for random fields (Adler (1981)), space-time extremes (Fedele (2012)) and associated stochastic wave groups (Fedele and Tayfun (2008)). Drawing on ERA-interim reanalysis (Dee et al. (2011)) we then study the statistical properties of *space-time extremes* of the Draupner storm. In concluding, we discuss the implications of these results on rogue-wave predictions.

2. Excess kurtosis of short-crested seas

Fedele (2014b) revisited Janssen's (2003) formulation for the total excess kurtosis C_4 of weakly nonlinear gravity waves in deep water. This comprises a dynamic component C_4^d due to nonlinear wave-wave interactions (Janssen and Bidlot (2009)) and a bound contribution $C_4^b = 6\mu^2$ induced by the characteristic crest-trough asymmetry of ocean waves (Tayfun (1980); Tayfun and Lo (1990); Tayfun and Fedele (2007); Fedele and Tayfun (2008); Fedele (2008)). For waves that are approximately narrowband and characterized with a Gaussian type directional spectrum, C_4^d is expressed as a sixfold integral that depends on time t, the BFI and R (Fedele (2014b)). Here, the parameter $R = \nu^2/2\sigma_\theta^2$ is a measure of short-crestedness of the dominant waves, with ν and σ_θ denoting spectral bandwidth and angular spreading (Janssen and Bidlot (2009); Mori et al. (2011)). The associated excess kurtosis growth rate can be solved analytically for narrowband waves (Fedele (2014b), see also appendix A). It is found that in the focusing regime ($0 < R < 1$) the dynamic excess kurtosis initially grows attaining a maximum $C_4^{\max}$ at the at the intrinsic time scale

$$\tau_c = 2\pi\nu^2 \frac{t_c}{T_0} = \frac{1}{\sqrt{3R}}, \qquad \text{or} \qquad \frac{t_c}{T_0} \sim \frac{0.13}{\nu\sigma_\theta} \tag{2}$$

given by the least-squares fit

$$\frac{C_4^{\max}(R)}{BFI^2} \approx \frac{b}{(2\pi)^2}\frac{1-R}{R+bR_0}, \qquad 0 \le R \le 1, \tag{3}$$

where $R_0 = \frac{3\sqrt{3}}{\pi}$ and $b = 2.48$. Eventually the excess dynamic kurtosis tends monotonically to zero as energy spreads directionally in accord with numerical simulations (Annenkov and Shrira (2009)). In the defocusing regime ($R > 1$) the dynamic excess kurtosis is always negative attaining a minimum at t_c given by (Janssen and Bidlot (2009))

$$C_4^{\min}\left(\frac{1}{R}\right) = -RC_4^{\max}(R), \qquad 0 \le R \le 1. \tag{4}$$

and then it tends to zero in the long time. Thus, the present theoretical predictions indicate a decaying trend for the dynamic excess kurtosis over large times.

For time scales $t \gtrsim 10t_c$ the wave wave field forgets its initial conditions and adjusts to a non-Gaussian state dominated by bound nonlinearities as the total kurtosis of surface elevations asymptotically approaches the bound component level (Annenkov and Shrira (2013, 2014)). In typical oceanic storms where dominant waves are characterized with $\nu \sim 0.2-0.4$ and $\sigma_\theta \sim 0.2-0.4$, this adjustment is rapid since the time scale $t_c/T_0 \sim O(1)$ with $T_0 \sim 10-14$ s and the dynamic kurtosis peak is negligible compared to the bound counterpart. For time scales of the order of or less than t_c the dynamic component can dominate and the wave field may experience rogue wave behavior induced by quasi-resonant interactions (Janssen (2003)). However, one can argue that the large excess kurtosis transient observed during the initial stage of evolution is a result of the unrealistic assumption that the initial wave field is homogeneous Gaussian. Oceanic wave fields are typically inohomogenous both in space and time.

In the left panel of Fig. (3), the preceding approximation is compared against the theoretical $C_4^{\max}$ for narrowband waves (Fedele (2014b), see also appendix A). Evidently, the latter is slightly larger than the maximum excess kurtosis derived by Janssen and Bidlot (2009), who have also used (3) but with $b = 1$. Their maximum follows by first taking the limit of the excess kurtosis at large times ($t = \infty$) and then solving the associated sixfold integral (Fedele (2014b)). Clearly, the dynamic excess kurtosis should vanish at large times. Janssen (personal communication, 2014) confirmed that Eq. (A3) holds and provided an alternative proof that C_4^d tends to zero as $t \to \infty$ using complex analysis. He also remarks that they are unresolved questions regarding the appropriate large-time behavior of the resonant function (Fedele (2014b)).

Further, in the focusing regime ($R < 1, \tau_c < 1/\sqrt{3}$), from (3)

$$\frac{C_4^{\max}(\tau_c)}{BFI^2} \approx \frac{b}{(2\pi)^2} \frac{-1+3\tau_c^2}{1+3bR_0\tau_c^2}. \tag{5}$$

Clearly, the maximum kurtosis becomes larger for longer time scales τ_c, as illustrated in the right panel of Fig. (3). In the defocusing regime ($R > 1, \tau_c > 1/\sqrt{3}$) the dynamic excess kurtosis is negative and the minimum value $C_4^{\min}$ can be computed from Eq. (4).

Drawing on ERA-interim reanalysis data, we now consider the Draupner storm event over the North Sea's area at the time of maximum development (Jan 2st 1995 UTC 00). For example, the top panel on the left of Fig. (2) shows the spatial distribution of the significant wave height $H_s = 4\sigma$ at the peak time. The maximum of H_s is about 8.5 m which is smaller than the observed 11.9 m (Karin Magnusson and Donelan (2013)). Indeed, it is well known that ERA understimates peak values and predict broader directional spectra because of the low spatial resolution of the data set, i.e. grid cell size $\sim 100^2$ km^2 and 60 vertical levels (Dee et al. (2011)). Nevertheless, such predictions provide leading order estimates of sea-state parameters that can be further refined in future studies using higher order resolution forecast models. For example, the top panels of Fig. (4) show the Gaussian adjustment time t_c/T_0 and the total excess kurtosis C_4. The dynamic and bound components are shown in the bottom panels of the same figure. Clearly,

$t_c \sim O(T_0) \sim 15$ seconds, indicating that nonlinear wave-wave interactions are negligible. Indeed, C_4^d is slightly negative indicating a defocusing wave regime due to the short-crestedness of the sea states, whereas the non-zero and positive bound component indicates that second order nonlinearities are dominant. Thus, in this regime statistical predictions of extreme waves can be based on the Tayfun (1980) model (Tayfun and Fedele (2007); Fedele and Tayfun (2008); Fedele (2008)) combined with Adler-Taylor's (2009) theory of Euler Characteristics for random fields. In the following, we will first present the theory of space-time extremes (Fedele (2012)) and then apply it to study the statistical properties of the Draupner freak wave event.

3. SPACE-TIME EXTREMES

In accord with ERA-interim reanalysis, in the time interval $D \sim 3$ hours and over the grid cell area $A \sim 100^2$ km^2 we can assume that the sea state is both stationary in time and homogenous in space. Then, the wave surface $\eta(\mathbf{x},t)$ can be modeled as a three-dimensional (3-D) homogeneous Gaussian random field over the space-time volume Ω defined by the area A and the time interval D, and $\mathbf{x} = (x,y)$ denotes the coordinate vector. Thus, the associated probability distributions at any points of the volume are the same and Gaussian. Drawing on Adler (1981), consider the Euler Characteristics (EC) of excursion sets of η defined as follows. Given a threshold z, the excursion set $U_\Omega(z)$ is the part of Ω within which η is above z:

$$U_\Omega(z) = \{(\mathbf{x},t) \in \Omega : \eta(\mathbf{x},t) > z\}.$$

In 1-D Gaussian processes, the EC simply counts the number of z-upcrossings, thus providing their generalization to higher dimensions. Indeed, for two dimensional (2-D) random fields, the EC counts the number of connected components minus the number of holes of the respective excursion set. In 3-D sets instead, the EC counts the number of connected volumetric components of the set, minus the number of holes that pass through it, plus the number of hollows inside. Further, the probability of exceedance that the global maximum of η over Ω, say η_{max}, exceeds z depends on the domain size and it is well approximated by the expected EC of the excursion set, provided that z is high (Adler (1981, 2000); Adler and Taylor (2009)). For an heuristic argument, as z increases the holes and hollows in the excursion set $U_\Omega(z)$ disappear until each of its connected components includes just one local maximum of η, and the EC counts the number of local maxima. For very large thresholds, the EC equals 1 if the global maximum exceeds the threshold and 0 otherwise. Thus, the EC of large excursion sets is a binary random variable with states 0 and 1, and, for large z,

$$\Pr\{\eta_{\max} > z\} = \Pr\{EC\,(U_\Omega(z)) = 1\} = \langle EC\,(U_\Omega(z))\rangle\,, \tag{6}$$

where angled brackets denote expectation. This heuristic identity has been proved rigorously to hold up to an error that is in general exponentially smaller than the expected EC approximation (Adler and Taylor (2009); Adler (2000)). For 3-D random fields, which are of interest in oceanic applications, the probability $P_{\mathrm{ST}}(\xi;A,D)$ that the maximum surface elevation $\eta_{\max}$ over the area A and during a time interval D exceeds the threshold ξH_s is given by (Adler and Taylor (2009))

$$\mathrm{P}_{\mathrm{ST}}(\xi;\mathrm{A},\mathrm{D}) = \Pr\{\eta_{\max} > \xi H_s\} = N_{\mathrm{ST}}(\xi;A,D)\mathrm{P}_R(\xi), \tag{7}$$

where

$$N_{\mathrm{ST}}(\xi_0;A,D) = 16M_3\xi_0^2 + 4M_2\xi_0 + M_1 \tag{8}$$

is interpreted as the average number of *space-time waves* occurring within the space-time volume Ω spanned by the area A and the time interval D and

$$P_{\mathrm{R}}(\xi) = \Pr\{h > \xi H_s\} = \exp(-8\xi^2) \tag{9}$$

is the Rayleigh exceedance probability of the crest height h of a *time wave* observed at a single point within the area A. Here, M_1,M_2 and M_3 are the average number of 1-D, 2-D and 3-D waves that can occur within the volume Ω (Fedele (2012)). They all depend upon the directional wave spectrum and are given in appendix A. Note that Piterbarg (1995) also derived an asymptotic expansion of the probability in (6) for large higher dimensional Gaussian maxima via generalized Rice (1944,1945) formulas.

A statistical indicator of the geometry of space-time extremes in the volume Ω is the wave dimension

$$\beta = 3 - \frac{4M_2\xi_0 + 2M_1}{16M_3\xi_0^2 + 4M_2\xi_0 + M_1}, \tag{10}$$

where $1 \leq \beta \leq 3$ (Fedele (2012)). The parameter represents a scale dimension of waves, i.e. the relative scale of a space-time wave with respect to the volume's size. In particular, if wave extremes are 3-D ($\beta > 2$) they are expected to occur within the volume Ω away from the boundaries, whereas the limiting case of 1-D time extremes ($\beta \sim 1$) occur for time waves observed at a single point. Furthermore, Fedele (2012) showed that *space-time extremes* are larger than *time extremes* in agreement with recent stereo measurements of oceanic sea states (Fedele et al. (2013)).

Drawing on ERA-interim reanalysis data, the bottom-left panel of Fig. (2) shows the map of the estimated wave dimension β for the North Sea's area at the Draupner storm peak time. Clearly, sea states are short-crested and extremes are roughly 3-D, indicating that the area is large compared to the mean wavelength. Thus, in accord with Boccotti's (2000) quasi-determinism theory a space-time extreme most likely coincides with the crest of a focusing wave group that passes through the area as discussed below.

4. Stochastic wave groups

Drawing on Fedele and Tayfun (2008); Fedele (2008), in accord with a second-order stochastic model of weakly nonlinear waves, the expected space-time dynamics nearby a large wave crest is that of a stochastic wave group, whose surface elevation is given by

$$\zeta_c = h_0\zeta_1 + \frac{h_0^2}{4\sigma}\zeta_2,$$

where h_0 is the linear crest amplitude distributed according to Eq. (7),

$$\zeta_1(\mathbf{X},T) = \Psi(\mathbf{X},T)$$

is the linear component,

$$\Psi(\mathbf{X},T) = \frac{\langle \eta(\mathbf{x},t)\eta(\mathbf{x}+\mathbf{X},t+T)\rangle}{\sigma^2} = \int \frac{S_1}{\sigma^2}\cos(\chi_1)\, d\omega_1 d\theta_1$$

is the space-time covariance of η (Boccotti (2000)) and

$$\zeta_2 = \int \frac{S_1 S_2}{\sigma^3}\left(A_{12}^{+}\cos(\chi_1+\chi_2) + A_{12}^{-}\cos(\chi_1-\chi_2)\right) d\omega_1 d\theta_1 d\omega_2 d\theta_2$$

is the second order component. Here, $S_j = S(\omega_j,\theta_j)$ and $\chi_j = \mathbf{k}_\mathrm{j}\cdot\mathbf{X} - \omega_j T$, where $\mathbf{X} = (X,Y)$ and $\mathbf{k}_\mathrm{j} = (k_j\sin\theta_j, k_j\cos\theta_j)$ with $k_j\tanh(k_j d) = \omega_j^2/g$ from linear dispersion, and the coefficients $A_{12}^{\pm}$ can be found in (Sharma and Dean (1979)). In the narrowband limit

$$\zeta_c = h_0\zeta_1 + \frac{h_0^2\omega_m^2}{2g}\left(\zeta_1^2 - \hat{\zeta}_1^2\right),$$

where $\hat{\zeta}_1$ is the Hilbert transform of ζ_1 with respect to time T and $\omega_m = m_{001}/m_{000}$ is the spectral mean frequency.

For generic sea states, the largest nonlinear crest amplitude is attained at the focusing point ($\mathbf{X} = \mathbf{0}, T = 0$) and given by

$$\xi = \xi_0 + 2\mu\xi_0^2, \tag{11}$$

where $\xi_0 = h_0/H_s$ and $\xi = h/H_s$ are the linear and nonlinear crest heights. The Tayfun wave steepness $\mu = \lambda_3/3$ relates to the skewness of surface elevations. For oceanic applications, Fedele and Tayfun (2008) proposed the approximation

$$\mu \sim \mu_a = \mu_m\left(1 - \nu + \nu^2\right) \tag{12}$$

where $\mu_m = \omega_m^2 \sigma / g$, $\omega_m = m_{001}/m_{000}$ is the mean spectral frequency and $\nu = \sqrt{m_{000} m_{002}/m_{001}^2 - 1}$ is the spectral bandwidth. Further, the wave trough following the large crest occurs at $t = T^*$, where T^* is the abscissa of the first miminum of the time covariance function (Boccotti (2000))

$$\psi(T) = \Psi(\mathbf{X} = \mathbf{0}, T) = \langle \eta(\mathbf{x}, t) \eta(\mathbf{x}, t + T) \rangle .$$

Note that second order nonlinearities do not affect the wave height since crests steepen as much as troughs shallow. Thus, the associated second order nonlinear crest-to-trought height is that of the linear group ζ_1, i.e.

$$H = h_0 (1 + \psi^*), \tag{13}$$

where $\psi^* = \psi(T^*)$ is the Boccotti's (2000) narrowbandedness parameter. Note that for narrow-band waves $\psi^* \to 1$. The left panels of Fig. (5) show the maps of the (top) Tayfun steepness μ_a and (bottom) Boccotti ψ^* estimated from ERA-interim reanalysis data at the time of maximum development of the Draupner storm. Clearly, $\psi^* \sim 0.75$ as the characteristic value of sea states dominated by wind waves (Boccotti (2000)) and the maximum wave steepness $\mu_a \sim 0.08$ typical of oceanic storms (Tayfun (2008)).

According to Fedele (2012), from (16) and (11) follow the expected space-time nonlinear crest height h_{ST} attained over the area A during a time interval D:

$$\xi_{ST} = \frac{h_{ST}}{H_s} = \xi_m + 2\mu\xi^2 + \frac{\gamma_e (1 + 4\mu\xi_m)}{16\xi_0 - \frac{32 M_3 \xi_m + 4 M_2}{16 M_3 \xi_m^2 + 4 M_2 \xi_m + M_1}},$$

where $\gamma_e = 0.577...$ is the Euler-Mascheroni constant and ξ_m is the most probable surface elevation value which, according to Gumbel (1958), satisfies

$$P_{ST}(\xi_m; A, D) = N_{ST}(\xi_m) P_R(\xi_\mathrm{m}) = 1.$$

The corresponding expected maximum nonlinear crest height h_T at a point during the time interval D is given by

$$\xi_T = \frac{h_T}{H_s} = \xi_m + 2\mu\xi_m^2 + \frac{\gamma_e(1+4\mu\xi_m)}{16\xi_m},$$

where, now, ξ_m satisfies $N_D P_R(\xi_m) = 1$ and $N_D = D/\bar{T}$ denotes the number of wave occurring during D and $\bar{T}$ is the mean up-crossing period (see appendix B). Fig. (5) shows the prediction of space-time extremes according to ERA-interm reanalysis of the Draupner storm at the significant wave height peak time. It is seen from the two top panels that the expected space-time extreme ξ_{ST} over the grid cell area $A \sim 100^2 \quad \text{km}^2$ during $D = 3$ hours is twice the expected maximum time crest extreme ξ_T at a single point (see also bottom-left panel for the map of the ratio ξ_{ST}/ξ_T). Further, the bottom-right panel shows that estimates of the steepness of such large crests do not violate the Stokes-Miche upper limit (Michell (1893)).

Clearly, in short-crested seas, in average, the number of space-time waves exceeding ξ_m is much larger than the number of time waves exceeding the same threshold at a point as it will be discussed later on. Their occurrence is sparse both in space and time in accord with a Poisson statistics (Aldous (1989); Piterbarg (1995)). It is natural to ask what is the probability that one of the large waves occurs within a smaller area as that covered by the Draupner's oil rig. The probability of this occurrence is not negligible and can be computed resorting to a Poisson Clumping Heuristics (Aldous (1989)) as presented below.

Given a crest-to-trough height $H = \alpha H_s$, the associated linear crest amplitude follows from (13) as

$$\xi_0(\alpha) = \frac{\alpha}{1+\psi^*} \tag{14}$$

and from (11) the nonlinear crest height

$$\xi(\alpha) = \xi_0(\alpha) + 2\mu\xi_0^2(\alpha) = \frac{\alpha}{1+\psi^*} + 2\mu\frac{\alpha^2}{(1+\psi^*)^2}. \tag{15}$$

Then, from (9) for a large threshold $\alpha \gg 1$ the '*time probability*' P_T that H exceeds αH_s during a time interval D is equal to the probability that the associated linear crest height exceeds ξ_0, that is

$$P_T(\alpha) = 1 - \exp(-N_D P_R(\xi_0)), \tag{16}$$

where N_D is the average number of time waves in the time interval D ((Gumbel 1958)). Similarly, for $\alpha \gg 1$ the '*space-time probability*' P_{ST} that H exceeds αH_s over an area A during D is given by Eq. (7) as

$$P_A(\alpha) = P_{ST}(\xi_0; A, D) = N_{ST}(\xi_0)P_R(\xi_0) \sim 1 - \exp(-N_{ST}(\xi_0)P_R(\xi_0)). \tag{17}$$

Clearly, in average the number of '*space-time waves*' exceeding ξ_0, i.e. $N_{ST}(\xi_0)P(\xi_0)$, is much larger than the number of '*time waves*' exceeding the same threshold at a point, i.e. $N_D P_R(\xi_0)$. Indeed, $N_{ST}(\xi_0) > N_D$ as $M_1 > N_D$ (see appendix B). However, what is the probability that one of the space-time waves occurs within a smaller area as that of the Draupner's oil rig fooprint ?

In short-crested seas, space-time waves larger than ξ_0 are Poisson distributed over a large area A and their average number λ per unit space-time volume is given by

$$\lambda = \frac{N_{ST}(\xi_0; A, D)P(\xi_0)}{AD}.$$

Thus, according to a Possion clumping heuristics (Aldous (1989)) the probability that one space-time wave occurs over a smaller area A_0 during the interval D is simply given by

$$P_{A_0}(\alpha) = 1 - \exp(-\lambda A_0 D) = 1 - \exp\left(-\frac{A_0}{A}N_{ST}(\xi_0; A, D)P(\xi_0)\right).$$

From (7),

$$P_{A_0}(\alpha) = 1 - \exp\left(-P_{ST}(\xi_0; A, D)\frac{A_0}{A}\right) \approx 1 - \exp\left(-P_{ST}(\xi_0; A_0, D)\right).$$

We remind that the measured Draupner wave has a crest-to-trough height $H = 2.15H_s$ and crest amplitude $h = 1.55H_s$. Based on ERA-interim reanalysis of the Draupner storm, for $\alpha = 2.15$ and $A \sim 100^2$ km^2 (the numerical grid cell area) the probability P_{A_0} that a *space-time wave* with $H > 2.15H_s$ occurs over a randomly chosen smaller area $A_0 = 50^2 m^2$ (the Draupner platform's footprint) is 10 to 40 times larger than the probability P_T that a *time wave* exceeds the same threshold at a single point. In particular, the open northern part of the North sea is more susceptible to larger extremes than the southern and central parts. This is seen in the top panels of Fig. (6) which show maps of the two abovementioned probabilities at the time of max development of the Draupner storm. The ratio P_{ST}/P_T is also shown in the bottom-left panel of the same figure. We conclude that it is more probable that a wave with $H > 2.15H_s$ hits an oil rig located in the northern part than in the central and southern parts. Further, the exceeded crest height threshold h/H_s is in the range of $1.35 - 1.55$ (see bottom-right panel) and estimates of the steepness of such large crests do not violate the Stokes-Miche upper limit.

Finally, the top panel of Fig. (7) compares the space-time probabilities P_{A_0} for areas $A_0 = 50^2, 100^2, 200^2$ m^2 and the time probability P_T at the Draupner site (58.2 N, 2.5 E). The threshold $H/H_s = 2.15$ is exceeded with probability $P_{A_0} \sim O(10^{-2} - 10^{-3})$, which is larger then the point probability $P_T \sim O(10^{-4})$. Further, the exceeded nonlinear crest height $h/H_s \sim 1.45$, in fair agreement with observations (Karin Magnusson and Donelan (2013)). As ERA-interim reanalysis in general understimates H_s peak values, we expect that the above probabilities are somewhat understimated as well.

5. Conclusions

These studies provide evidence that freak wave behavior may be a manifestation of the space-time properties of oceanic fields. Over larger areas (compared to the mean wavelength) a space-time extreme most likely coincides with the maximum crest of a stochastic wave group that passes through the area, in accord with Boccotti's (2000) quasi-determinism theory. Estimates of the steepness of such large crests do not violate the Stokes-Miche upper limit.

Third-order quasi-resonant interactions do not appear to play a significant role in wave growth. The associated large excess kurtosis transient observed during the initial stage of wave evolution is a result of the unrealistic assumption that the initial wave field is homogeneous and Gaussian. Oceanic wave fields are typically inohomogenous both in space and time. If the wind is sufficiently stationary and the underlying environmental conditions do not change, a random wave field forgets its initial conditions and adjusts to a non-Gaussian state dominated by bound nonlinearities (Annenkov and Shrira (2013, 2014)). In typical oceanic storms where dominant waves are characterized by $\nu \sim 0.2-0.4$ and $\sigma_\theta \sim 0.2-0.4$, this adjustment is rapid since the time scale $t_c/T_0 \sim O(1)$ with $T_0 \sim 10-14$ s and the dynamic kurtosis peak is negligible compared to the bound counterpart. In this regime, statistical predictions of extreme waves can be based on the Tayfun (1980) model (Tayfun and Fedele (2007); Fedele and Tayfun (2008); Fedele (2008)).

Spatial and temporal inhomogeneity of the wave field should be accounted for. For example, in a storm the significant wave height varies both in space and time and the short-term prediction of extremes should be modified accordingly (see, e.g. Fedele (2012)). Finally, further studies based on higher resolution forecast models are desirable.

6. Acknowledgments

FF is grateful to Jean Bidlot for providing the ERA-interim data of the Draupner storm and for the support in the data analysis. FF also thanks Michael Banner, George Forristall, Peter Janssen, Victor Shrira and M. Aziz Tayfun for discussions on nonlinear wave statistics and random wave fields. Finally, a special thanks goes to M. Aziz Tayfun and Philip J. Roberts for revising an early draft of the manuscript.

APPENDIX A

Dynamic Excess Kurtosis

For narrowband waves in deep waters, the evolution of the dynamic excess kurtosis from initial Gaussian conditions is given by (Fedele (2014b))

$$C_4^d = BFI^2 J(\tau, R) \tag{A1}$$

where

$$J(\tau;R) = 2\,\mathrm{Im}\int_0^{\tau} \frac{1}{\sqrt{1-2i\alpha+3\alpha^2}\sqrt{1+2iR\alpha+3R^2\alpha^2}}d\alpha. \tag{A2}$$

The maximum is attained at $\tau = \tau_c$ (see Eq. (2)) and given by

$$C_4^{\max}(R) = BFI^2 J_p(R), \tag{A3}$$

where

$$J_p(R) = J\left(\frac{1}{\sqrt{3R}};R\right) = \mathrm{Im}\int_0^{\frac{1}{\sqrt{3R}}} \frac{2}{\sqrt{1-2i\alpha+3\alpha^2}\sqrt{1+2iR\alpha+3R^2\alpha^2}}d\alpha,$$

and $\mathrm{Im}(a)$ denotes the imaginary part of a.

APPENDIX B

Space-Time Statistical Parameters

For space-time extremes, the coefficients in Eq. (8) are given by (Baxevani and Rychlik (2006); Fedele (2012))

$$M_3 = 2\pi \frac{D}{\overline{T}} \frac{\ell_x}{\overline{L_x}} \frac{\ell_y}{\overline{L_y}} \alpha_{xyt},$$

$$M_2 = \sqrt{2\pi} \left(\frac{D}{\overline{T}} \frac{\ell_x}{\overline{L_x}} \sqrt{1-\alpha_{xt}^2} + \frac{D}{\overline{T}} \frac{\ell_y}{\overline{L_y}} \sqrt{1-\alpha_{yt}^2} + \frac{\ell_x}{\overline{L_x}} \frac{\ell_y}{\overline{L_y}} \sqrt{1-\alpha_{xy}^2} \right),$$

$$M_1 = N_D + N_x + N_y,$$

where

$$N_D = \frac{D}{\overline{T}}, \qquad N_x = \frac{\ell_x}{\overline{L_x}}, \qquad N_y = \frac{\ell_y}{\overline{L_y}}$$

are the average number of waves occurring during the time interval D and along the x and y sides of length ℓ_x and ℓ_y respectively. They all depend on the mean period $\overline{T}$, mean wavelengths $\overline{L_x}$ and $\overline{L_Y}$ in x and y directions:

$$\overline{T} = 2\pi \sqrt{\frac{m_{000}}{m_{002}}}, \qquad \overline{L_x} = 2\pi \sqrt{\frac{m_{000}}{m_{200}}}, \qquad \overline{L_y} = 2\pi \sqrt{\frac{m_{000}}{m_{020}}}$$

and

$$\alpha_{xyt} = \sqrt{1 - \alpha_{xt}^2 - \alpha_{yt}^2 - \alpha_{xy}^2 + 2\alpha_{xt}\alpha_{yt}\alpha_{xy}}.$$

Here,

$$m_{ijk} = \iint k_x^i k_y^j f^k S(f,\theta) df d\theta$$

are the moments of the directional spectrum and

$$\alpha_{xt} = \frac{m_{101}}{\sqrt{m_{200}m_{002}}}, \qquad \alpha_{yt} = \frac{m_{011}}{\sqrt{m_{020}m_{002}}}, \qquad \alpha_{xy} = \frac{m_{110}}{\sqrt{m_{200}m_{020}}}.$$

References

Adcock, T., P. Taylor, S. Yan, Q. Ma, and P. Janssen, 2011: Did the draupner wave occur in a crossing sea? *Proceedings of the Royal Society A: Mathematical, Physical and Engineering Science*, rspa20110049.

Adler, R. J., 1981: *The geometry of random fields*, Vol. 62. Siam.

Adler, R. J., 2000: On excursion sets, tube formulas and maxima of random fields. *Annals of Applied Probability*, 1–74.

Adler, R. J., and J. E. Taylor, 2009: *Random fields and geometry*, Vol. 115. Springer Monographs in Mathematics.

Aldous, D., 1989: Probability approximations via the poisson clumping heuristic. Springer, New York.

Ankiewicz, A., N. Devine, and N. Akhmediev, 2009: Are rogue waves robust against perturbations? *Physics Letters A*, **373**, 3997–4000.

Annenkov, S. Y., and V. I. Shrira, 2009: Evolution of kurtosis for wind waves. *Geophysical Research Letters*, **36 (13)**, 1944–8007, doi:10.1029/2009GL038613, URL http://dx.doi.org/10.1029/2009GL038613.

Annenkov, S. Y., and V. I. Shrira, 2013: Large-time evolution of statistical moments of wind–wave fields. *Journal of Fluid Mechanics*, **726**, 517–546, doi:10.1017/jfm.2013.243, URL http://journals.cambridge.org/article_S0022112013002437.

Annenkov, S. Y., and V. I. Shrira, 2014: Evaluation of skewness and kurtosis of wind waves parameterized by jonswap spectra. *Journal of Physical Oceanography*, **44 (6)**, 1582–1594, doi:10.1175/JPO-D-13-0218.1, URL http://dx.doi.org/10.1175/JPO-D-13-0218.1.

Baxevani, A., and I. Rychlik, 2006: Maxima for gaussian seas. *Ocean Engineering*, **33 (7)**, 895 – 911, doi:http://dx.doi.org/10.1016/j.oceaneng.2005.06.006, URL http://www.sciencedirect.com/science/article/pii/S0029801805001952.

Boccotti, P., 2000: *Wave Mechanics for Ocean Engineering*. Elsevier Sciences, Oxford, 496 pp.

Chabchoub, A., N. Hoffmann, M. Onorato, and N. Akhmediev, 2012: Super rogue waves: Observation of a higher-order breather in water waves. *Phys. Rev. X*, **2**, 011 015, doi:10.1103/PhysRevX.2.011015, URL http://link.aps.org/doi/10.1103/PhysRevX.2.011015.

Chabchoub, A., N. P. Hoffmann, and N. Akhmediev, 2011: Rogue wave observation in a water wave tank. *Phys. Rev. Lett.*, **106**, 204 502, doi:10.1103/PhysRevLett.106.204502, URL http://link.aps.org/doi/10.1103/PhysRevLett.106.204502.

Christou, M., and K. Ewans, 2014: Field measurements of rogue water waves. *Journal of Physical Oceanography*, **44 (9)**, 2317–2335, doi:10.1175/JPO-D-13-0199.1, URL http://dx.doi.org/10.1175/JPO-D-13-0199.1.

Dee, D. P., and Coauthors, 2011: The era-interim reanalysis: configuration and performance of the data assimilation system. *Quarterly Journal of the Royal Meteorological Society*, **137 (656)**, 553–597, doi:10.1002/qj.828, URL http://dx.doi.org/10.1002/qj.828.

Dyachenko, A. I., and V. E. Zakharov, 2011: Compact Equation for Gravity Waves on Deep Water. *JETP Lett.*, **93 (12)**, 701–705.

Dysthe, K. B., 1979: Note on a modification to the nonlinear Schrödinger equation for application to deep water. *Proc. R. Soc. Lond. A*, **369**, 105–114.

Dysthe, K. B., H. E. Krogstad, and P. Muller, 2008: Oceanic rogue waves. *Annual Review of Fluid Mechanics*, **40**, 287–310.

Fedele, F., 2008: Rogue waves in oceanic turbulence. *Physica D*, **237**, 2127–2131.

Fedele, F., 2012: Space–time extremes in short-crested storm seas. *Journal of Physical Oceanography*, **42 (9)**, 1601–1615, doi:10.1175/JPO-D-11-0179.1, URL http://dx.doi.org/10.1175/JPO-D-11-0179.1.

Fedele, F., 2014a: On certain properties of the compact zakharov equation. *Journal of Fluid Mechanics*, **748**, 692–711, doi:10.1017/jfm.2014.192, URL http://journals.cambridge.org/article_S002211201400192X.

Fedele, F., 2014b: On the kurtosis of ocean waves in deep water. *arXiv preprint arXiv:1412.8231*.

Fedele, F., A. Benetazzo, G. Gallego, P.-C. Shih, A. Yezzi, F. Barbariol, and F. Ardhuin, 2013: Space–time measurements of oceanic sea states. *Ocean Modelling*, **70**, 103–115.

Fedele, F., and M. A. Tayfun, 2008: On nonlinear wave groups and crest statistics. *J. Fluid Mech*, **620**, 221–239.

Forristall, G. Z., 2011: Maximum crest heights under a model tlp deck. *ASME 2011 30th International Conference on Ocean, Offshore and Arctic Engineering*, American Society of Mechanical Engineers, 571–577.

Gumbel, E. J., 1958: *Statistics of extremes*. 1–373, Columbia University Press, New York.

Haver, S., 2001: Evidences of the existence of freak waves. *Rogue Waves*, 129–140.

Haver, S., 2004: A possible freak wave event measured at the draupner jacket january 1 1995. *Rogue waves 2004*, 1–8.

Janssen, P. A. E. M., 2003: Nonlinear four-wave interactions and freak waves. *Journal of Physical Oceanography*, **33 (4)**, 863–884.

Janssen, P. A. E. M., 2014: Notes on kurtosis evolution for 2d wave propagation. Memorandum Research Department 60.9/PJ/0387, ECMWF.

Janssen, P. A. E. M., and J. R. Bidlot, 2009: On the extension of the freak wave warning system and its verification. Tech. Memo 588, ECMWF.

Karin Magnusson, A., and M. A. Donelan, 2013: The andrea wave characteristics of a measured north sea rogue wave. *Journal of Offshore Mechanics and Arctic Engineering*, **135 (3)**, 031 108–031 108, URL http://dx.doi.org/10.1115/1.4023800.

Kharif, C., and E. Pelinovsky, 2003: Physical mechanisms of the rogue wave phenomenon. *European Journal of Mechanics - B/Fluids*, **22 (6)**, 603 – 634, doi:http://dx.doi.org/10.1016/j.euromechflu.2003.09.002, URL http://www.sciencedirect.com/science/article/pii/S0997754603000724.

Lighthill, M. J., 1965: Contributions to the theory of waves in non-linear dispersive systems. *IMA Journal of Applied Mathematics*, **1 (3)**, 269–306, doi:10.1093/imamat/1.3.269, URL http://imamat.oxfordjournals.org/content/1/3/269.abstract, http://imamat.oxfordjournals.org/content/1/3/269.full.pdf+html.

Michell, J. H., 1893: On the highest waves in water. *Philos. Mag.*, **5**, 430—437.

Mori, N., and P. A. E. M. Janssen, 2006: On kurtosis and occurrence probability of freak waves. *Journal of Physical Oceanography*, **36 (7)**, 1471–1483, doi:10.1175/JPO2922.1, URL http://dx.doi.org/10.1175/JPO2922.1.

Mori, N., M. Onorato, and P. A. E. M. Janssen, 2011: On the estimation of the kurtosis in directional sea states for freak wave forecasting. *Journal of Physical Oceanography*, **41 (8)**, 1484–1497, doi:10.1175/2011JPO4542.1, URL http://dx.doi.org/10.1175/2011JPO4542.1.

Onorato, M., D. Proment, and A. Toffoli, 2010: Freak waves in crossing seas. *The European Physical Journal-Special Topics*, **185 (1)**, 45–55.

Onorato, M., and Coauthors, 2009: Statistical properties of mechanically generated surface gravity waves: a laboratory experiment in a three-dimensional wave basin. *Journal of Fluid Mechanics*, **627**, 235–257, doi:10.1017/S002211200900603X, URL http://journals.cambridge.org/article_S002211200900603X.

Osborne, A., 2010: *Nonlinear ocean waves and the inverse scattering transform*, Vol. 97. Elsevier, 917 pp. pp., URL http://scholar.google.com/scholar?hl=en&btnG=Search&q=intitle:Nonlinear+ocean+waves+and+the+inverse+scattering+transform#1.

Osborne, A. R., M. Onorato, and M. Serio, 2000: The nonlinear dynamics of rogue waves and holes in deep-water gravity wave trains. *Phys. Lett. A*, **275 (5-6)**, 386–393, doi:10.1016/S0375-9601(00)00575-2, URL http://linkinghub.elsevier.com/retrieve/pii/S0375960100005752.

Peregrine, D. H., 1983: Water waves, nonlinear Schrödinger equations and their solutions. *Journal of the Australian Mathematical Society Series B*, **25**, 16–43.

Piterbarg, V. I., 1995: *Asymptotic methods in the theory of Gaussian processes and fields*, Vol. 148. AMS ser. Translations of Mathematical Monographs.

Rice, S. O., 1944: Mathematical analysis of random noise. *Bell Syst. Tech. J.*, **23 (282–332)**.

Rice, S. O., 1945: Mathematical analysis of random noise. *Bell Syst. Tech. J.*, **24 (46–156)**.

Rosenthal, W., and S. Lehner, 2008: Rogue waves: Results of the maxwave project. *Journal of Offshore Mechanics and Arctic Engineering*, **130 (2)**, 021 006–021 006, URL http://dx.doi.org/10.1115/1.2918126.

Sharma, J. N., and R. G. Dean, 1979: *Development and evaluation of a procedure for simulating a random directional second order sea surface and associated wave forces*. 20, University of Delaware.

Shemer, L., and S. Alperovich, 2013: Peregrine breather revisited. *Physics of Fluids*, **25**, 051 701.

Shemer, L., and D. Liberzon, 2014: Lagrangian kinematics of steep waves up to the inception of a spilling breaker. *Physics of Fluids*, **26 (1)**, 016 601, doi:http://dx.doi.org/10.1063/1.4860235, URL http://scitation.aip.org/content/aip/journal/pof2/26/1/10.1063/1.4860235.

Shemer, L., and A. Sergeeva, 2009: An experimental study of spatial evolution of statistical parameters in a unidirectional narrow-banded random wavefield. *Journal of Geophysical Research: Oceans*, **114 (C1)**, 2156–2202, doi:10.1029/2008JC005077, URL http://dx.doi.org/10.1029/2008JC005077.

Slunyaev, A., E. Pelinovsky, A. Sergeeva, A. Chabchoub, N. Hoffmann, M. Onorato, and N. Akhmediev, 2013: Super-rogue waves in simulations based on weakly nonlinear and fully nonlinear hydrodynamic equations. *Phys. Rev. E*, **88**, 012 909, doi:10.1103/PhysRevE.88.012909, URL http://link.aps.org/doi/10.1103/PhysRevE.88.012909.

Slunyaev, A. V., and V. I. Shrira, 2013: On the highest non-breaking wave in a group: fully nonlinear water wave breathers versus weakly nonlinear theory. *Journal of Fluid Mechanics*, **735**, 203–248, doi:10.1017/jfm.2013.498, URL http://journals.cambridge.org/article_S0022112013004989.

Tayfun, M. A., 1980: Narrow-band nonlinear sea waves. *Journal of Geophysical Research: Oceans*, **85 (C3)**, 1548–1552, doi:10.1029/JC085iC03p01548, URL http://dx.doi.org/10.1029/JC085iC03p01548.

Tayfun, M. A., 2008: Distributions of envelope and phase in wind waves. *Journal of Physical Oceanography*, **38 (12)**, 2784–2800, doi:10.1175/2008JPO4008.1, URL http://dx.doi.org/10.1175/2008JPO4008.1.

Tayfun, M. A., and F. Fedele, 2007: Wave-height distributions and nonlinear effects. *Ocean Engineering*, **34 (11–12)**, 1631 – 1649, doi:http://dx.doi.org/10.1016/j.oceaneng.2006.11.006, URL http://www.sciencedirect.com/science/article/pii/S0029801807000431.

Tayfun, M. A., and J. Lo, 1990: Nonlinear effects on wave envelope and phase. *J. Waterway, Port, Coastal and Ocean Eng.*, **116**, 79–100.

Toffoli, A., O. Gramstad, K. Trulsen, J. Monbaliu, E. Bitner-Gregersen, and M. Onorato, 2010: Evolution of weakly nonlinear random directional waves: laboratory experiments and numerical simulations. *Journal of Fluid Mechanics*, **664**, 313–336, doi:10.1017/S002211201000385X, URL http://journals.cambridge.org/article_S002211201000385X.

LIST OF FIGURES

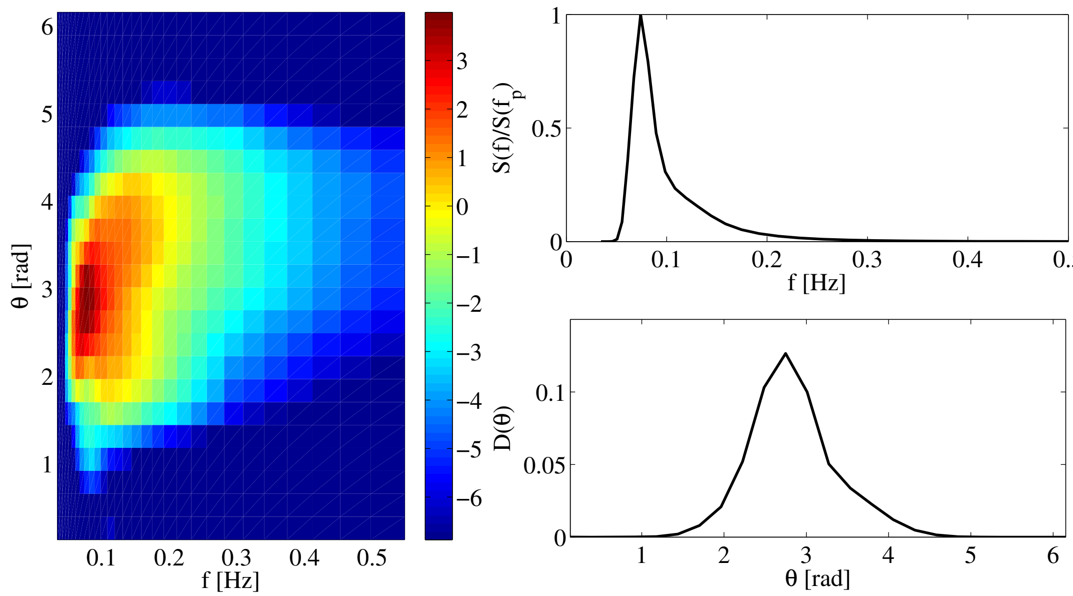

FIG. 1. Draupner storm: ERA-interm (left) directional spectrum (log scale) at the Draupner site (58.2 N,2.5 E) at the time of maximum development of the storm (Jan 2st 1995 UTC 00) and (top-right) wave frequency spectrum $S(f)/S(f_p)$ and (bottom-right) angular dispersion $\sigma^2 D(\theta) = \int S(f,\theta) df$, where σ is the standard deviation of surface elevations and f_p the dominant frequency. Direction $\theta = 0$ means going to the north and $\theta = \pi/2$ to the east (Oceanographic convention).

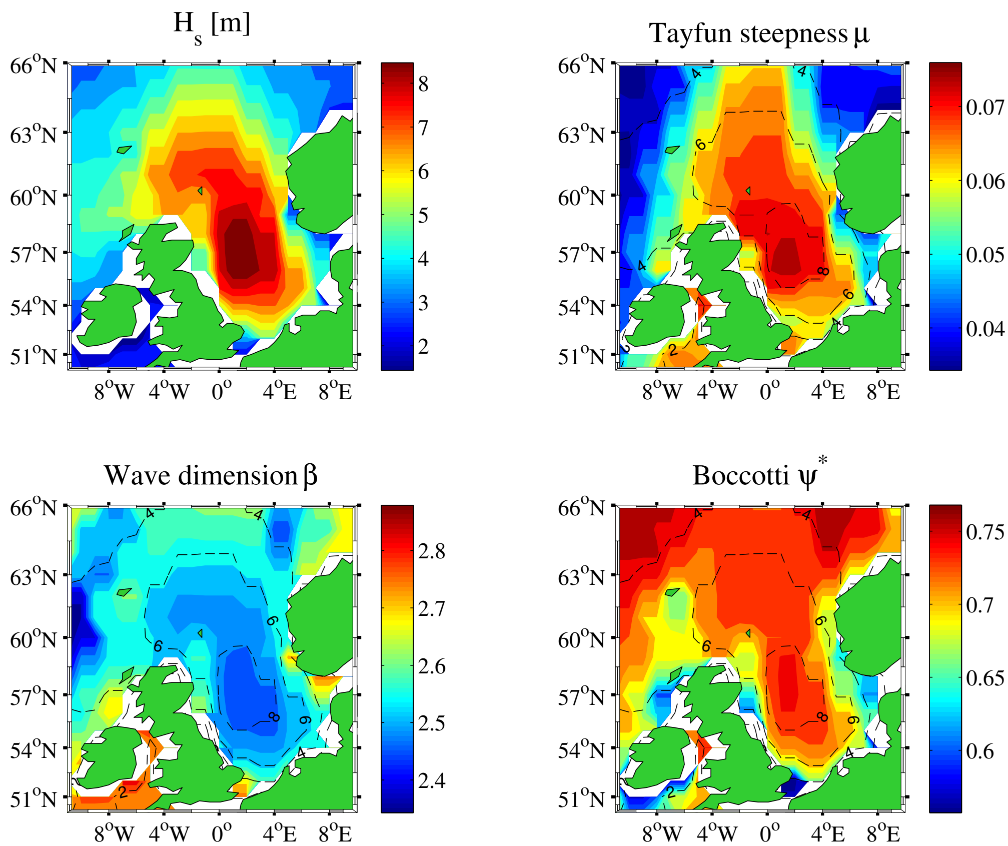

FIG. 2. ERA-interim reanalysis at the time of maximum development of the Draupner storm (Jan 2st 1995 UTC 00). Top panels: (left) significant wave height $H_s = 4\sigma$ and (right) Tayfun wave steepness μ (Eq. (12)). Bottom panels: (left) wave dimension β (Eq. (10)) and (right) narrowbandedness Boccotti parameter ψ^*. Dashed lines are H_s contours.

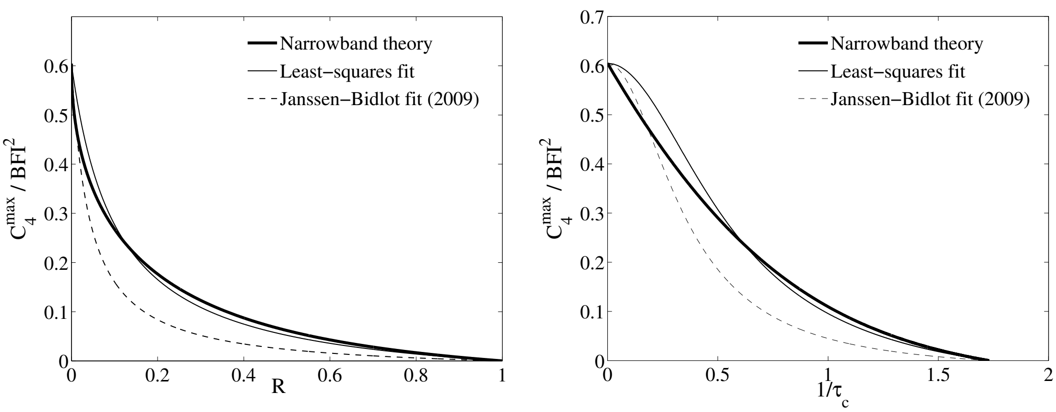

FIG. 3. Maximum dynamic excess kurtosis $C_4^{\max}$ as a function of (left) R and (right) $1/\tau_c$: (bold line) present theoretical prediction, (thin line) least-squares fit from Eq. (3) ($b = 2.48$) and (dash line) Janssen-Bidlot (2009) fit ($b = 1$).

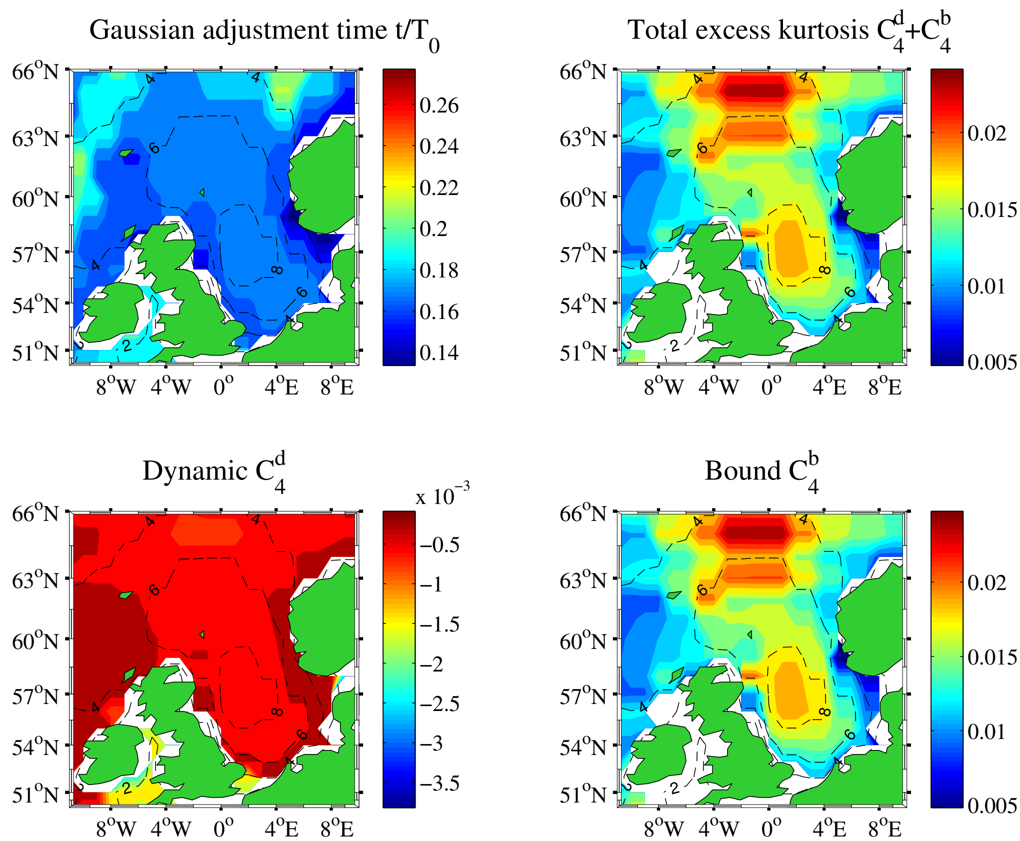

FIG. 4. ERA-interim reanalysis at the time of maximum development of the Draupner storm (Jan 2st 1995 UTC 00). Top panels: (left) Gaussian adjustment time t_c/T_0 (Eq. (2)) and (right) total excess kurtosis $C_4 = C_4^d + C_4^b$. Bottom panels: (left) dynamic excess kurtosis C_4^d (Eq. (3)) and (right) bound excess kurtosis $C_4^b = 18\mu^2$. Dashed lines are H_s contours.

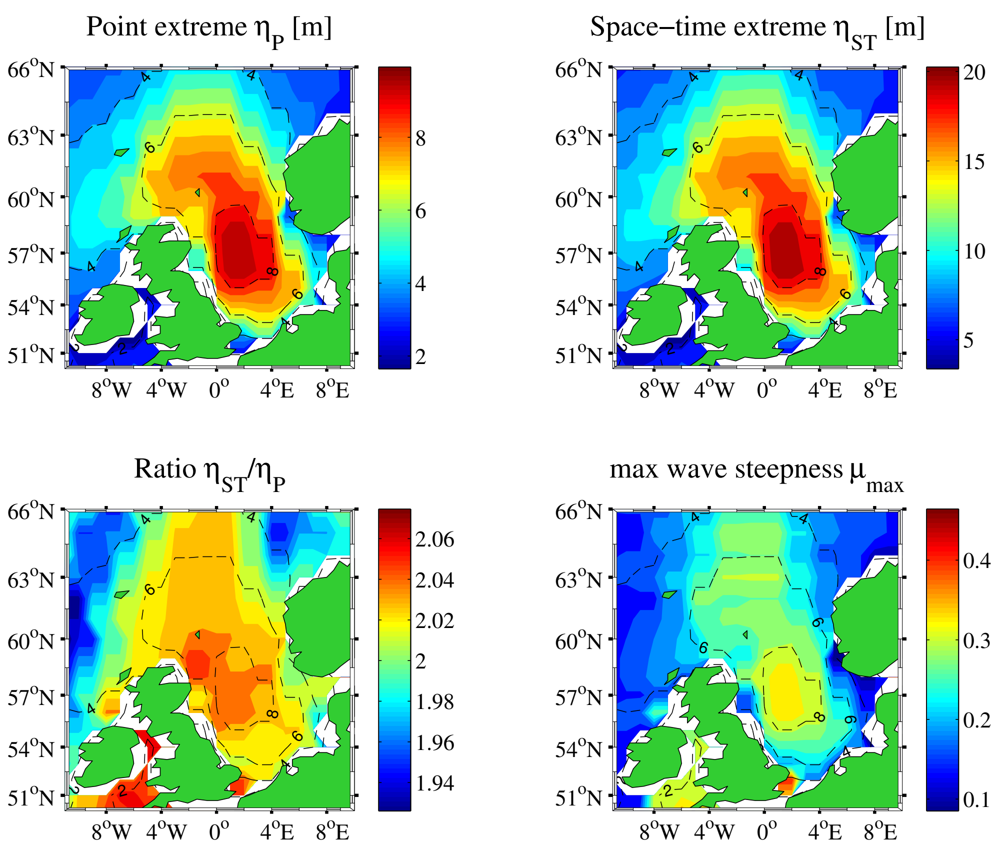

FIG. 5. ERA-interm reanalysis of the Draupner storm at the time of maximum development (Jan 2st 1995 UTC 00). Top panels: (left) expected maximum time crest extreme η_T at a single point and (right) corresponding space-time extreme η_{ST} expected over the grid cell size $\sim 100^2 km^2$ during $D = 3$ hours. Bottom panels: (left) ratio η_{ST}/η_T and (right) maximum expected wave steepness. Dashed lines are H_s contours.

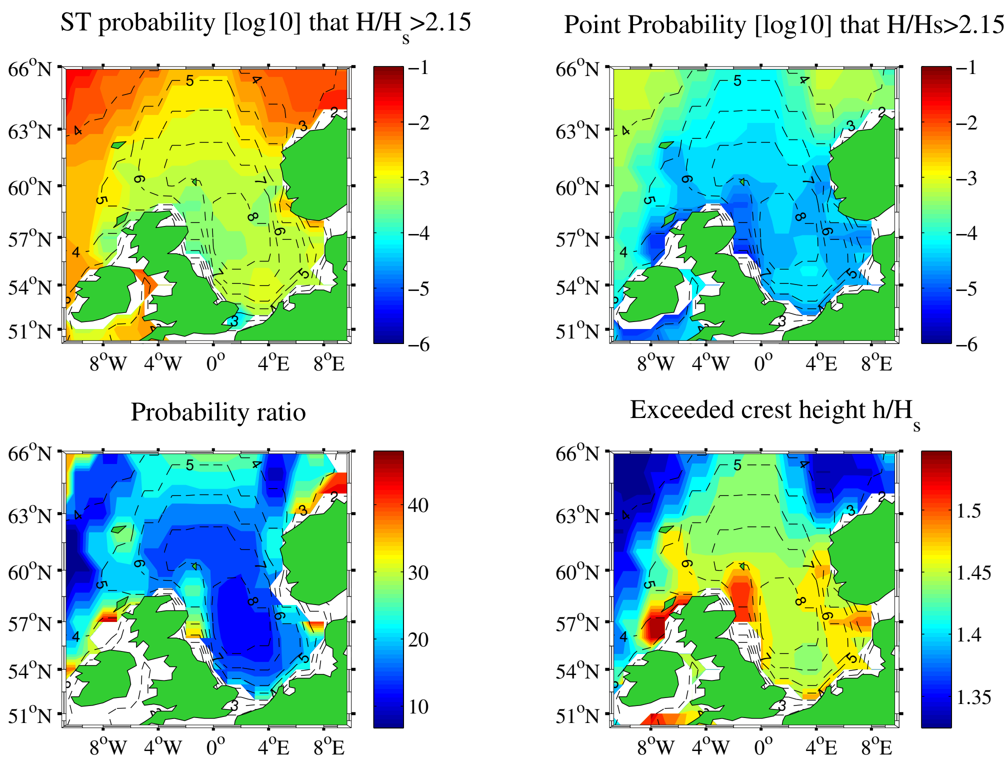

FIG. 6. ERA-interim reanalysis at the time of maximum development of the Draupner storm (Jan 2st 1995 UTC 00). Top panels: (left) probability $P_{ST}(H/H_s;A_0,D)$ (log_{10} units) that a wave with $H/H_s > 2.15$ occurs over an area $\sim A_0 = 50^2 m^2$ during $D = 3$ hours and (right) corresponding probability $P_T(H/H_s;D)$ that the same wave occurs at a single point in time. Bottom panels: (left) probability ratio P_{ST}/P_T and (right) exceeded nonlinear crest height h/H_s. Dashed lines are H_s contours.

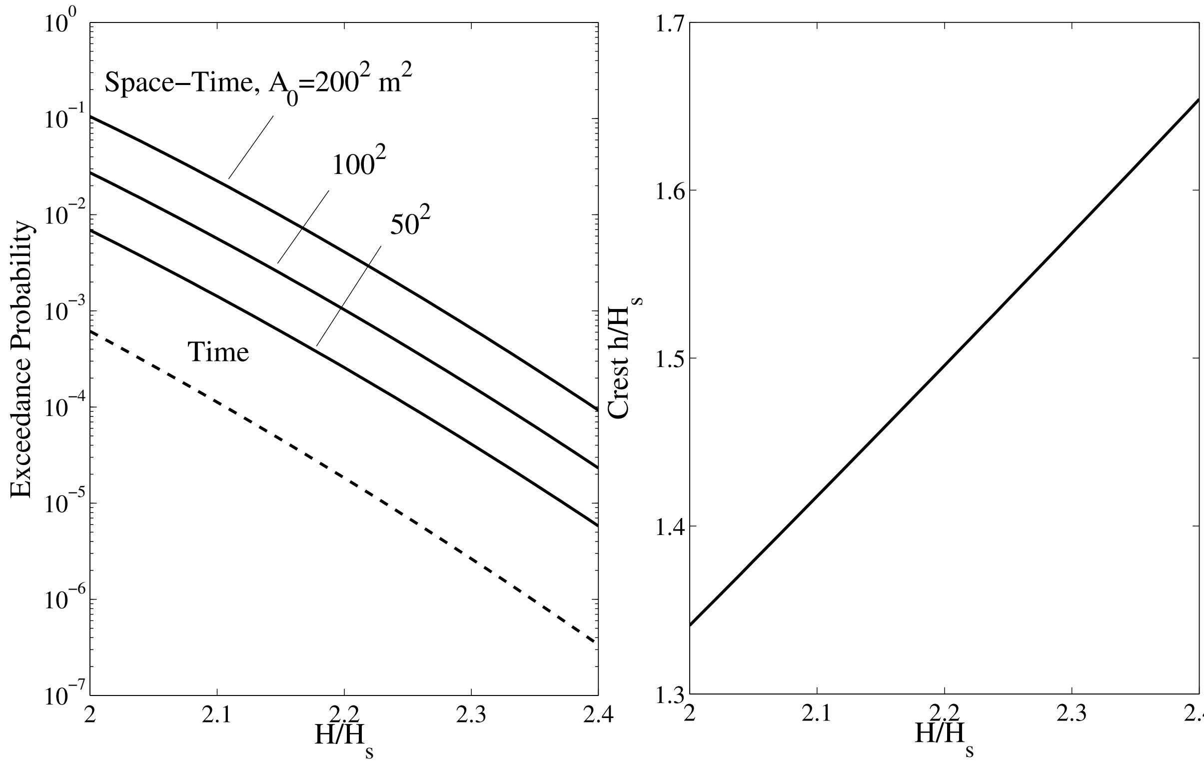

FIG. 7. ERA-interim reanalysis at the time of maximum development of the Draupner storm (Jan 2st 1995 UTC 00) at the platform site (58.2 N, 2.5 E). Left: space-time probability $P_{ST}(H/H_s;A_0,D)$ for $A_0 = 50^2, 100^2, 200^2\ m^2$ and corresponding time probability $P_T(H/H_s;D)$ as a function of H/H_s and $D = 3$ hours. Right: exceeded second order nonlinear crest height h/H_s as a function of H/H_s.